Origin of the structures in the ^{12}C(^{16}O,α) reaction: Dominance of ^{20}Ne* and ^{16}O* sequential α-decay processes

T. Murakami,* E. Ungricht,† N. Takahashi,‡ Y.-W. Lui, Y. Mihara,§ R. E. Neese,
E. Takada,** D. M. Tanner, R. E. Tribble, and K. Nagatani*

Cyclotron Institute, Texas A&M University, College Station, Texas 77843

(Received 29 August 1983)

A series of experiments was carried out on the ^{12}C(^{16}O,α) reaction to search for the population of molecular resonances as final state interactions. Contrary to our expectation, no positive evidence was found in α-^{12}C coincidence measurements for molecular states. The experimental configuration was arranged to selectively observe events corresponding to decays into the ^{12}C+^{12}C resonance channel. A study of the incident energy dependence of the ^{12}C(^{16}O,α) reaction clearly indicates the importance of sequential processes in the α-particle yield. In particular, the process where the incident ^{16}O picks up an α forming ^{20}Ne* resonances and then decays back to α+^{16}O can reasonably explain most of observed structures in the inclusive α spectra. The sequential process caused by the inelastic excitation of ^{16}O to ^{16}O*→α+^{12}C can also contribute to the broad peaks observed in the inclusive spectra, but only in the high excitation region.

I. INTRODUCTION

Since Lazzarini et al.[1] first suggested that nuclear molecular resonances might be formed as final states in the ^{12}C(^{16}O,α)^{24}Mg reaction at ^{16}O incident energies between 62 and 100 MeV, several experimental and theoretical investigations have been performed on this reaction. Recently, Nagatani et al.[2] studied the same reaction at the higher incident energy of $E(^{16}$O$)=145$ MeV and observed prominent structures on an underlying continuum background in the range of $E_x(^{24}$Mg$)=30-56$ MeV. The observed structures were thought to be the result of a direct transfer reaction to the high-spin members of the ^{12}C + ^{12}C nuclear molecular resonances. This interpretation was based on (1) the close correlation between the excitation energies of the structures in the ^{24}Mg system and the ^{12}C-^{12}C nuclear molecular states (12^+), (14^+), (16^+), and (18^+); (2) the structures showed very forward peaked angular distribution; and (3) similar structures were absent in the ^{13}C(^{16}O,α) reaction. While a simple theory of kinematical matching conditions also supported this interpretation,[3] several experimental results cast some doubt on it. There have been numerous investigations of this problem, but the situation is complicated and the general understanding is unclear. Below, we summarize the experimental situation.

Rae et al.[4] measured the ^{12}C(^{16}O,α^{12}C)^{12}C and the ^{13}C(^{16}O,α^{12}C)^{13}C correlations at an ^{16}O incident energy of 140 MeV. Since the high-spin molecular resonances observed in the ^{12}C + ^{12}C system are naively considered to have large partial widths for the decay into ^{12}C(g.s.) + ^{12}C(g.s.) and ^{12}C(g.s.) + ^{12}C(2^+) channels, the coincidence measurement is a direct attempt to confirm the formation of molecular states. The result was negative; no evidence for the ^{12}C + ^{12}C resonance decay was found. However, $\alpha + ^{12}$C final state resonances were clearly observed. Based on this observation, Rae et al. offered the sequential decay process of ^{16}O* as one possible origin

of the structures in the inclusive spectrum. But without a quantitative estimate of the intensity of the structures coming from ^{16}O* in a singles spectrum, the supposition could not be confirmed. It should further be noted that the relative difference in the ^{16}O*→^{12}C + α processes observed with the ^{12}C and ^{13}C targets was not more than a factor of 2, which clearly contradicted the inclusive data that showed an absence of structures in the singles α spectrum from the ^{13}C target.

The same interpretation, a sequential decay process of ^{16}O*, was also proposed by Branford et al.[5] They measured the total widths and α-decay branching ratios of the peaks in the inclusive α spectrum of the ^{12}C(^{16}O,α)^{24}Mg reaction with good energy resolution in the bombarding energy range of 60 to 100 MeV. It turned out that peaks observed in the ^{24}Mg excitation energy $E_x=20-30$ MeV did not have the same widths and decay branching ratios that the known molecular states in ^{24}Mg have. Based on these results, they speculated that the structures observed in the much higher ^{24}Mg excitation energy range (30−50 MeV) might come from the sequential decay of ^{16}O*.

Systematic measurements of the (^{16}O,α) reaction on ^{14}N, ^{16}O, and ^{20}Ne targets performed by Takahashi et al.[6] revealed that prominent broad peaks were observed in the reactions on the ^{16}O and ^{20}Ne targets, while they were absent with the ^{14}N target. With this information, it is difficult to believe that the sequential α decay of ^{16}O* is responsible for the structures in the inclusive α spectra.

Meanwhile, Szanto de Toledo et al.[7] proposed that the structures are an extension of the ^{24}Mg yrast states that are populated by the high-spin selectivity of α-particle evaporation from the ^{28}Si compound nucleus. The yrast states would not have a large ^{12}C + ^{12}C configuration and hence they could not be observed in the decay experiments. Takahashi et al.[8] performed a measurement of the ^{14}N(^{14}N,α) reaction at an $E_{lab}(^{14}$N$)=111$ MeV, which leads to the same compound nucleus ^{28}Si as the ^{12}C(^{16}O,α) reaction at $E_{lab}(^{16}$O$)=145$ MeV. Contrary to the sugges-

tion of Szanto de Toledo *et al.*, the resultant α inclusive spectrum did not show the distinct structures which were observed in the $^{12}C(^{16}O,\alpha)$ reaction. A theoretical analysis using the Hauser-Feshbach formalism with a normal level density formula shows that α particles evaporated from the ^{28}Si compound nucleus only produce smooth spectra and that the observed continuum background might come mainly from the compound process. However, in a recent study of the compound nucleus mechanism in the $^{12}C(^{16}O,\alpha)$ reaction at high energies, Cormier *et al.*[9] suggested that the absence of structures in the $^{14}N(^{14}N,\alpha)$ reaction can be understood by the high-spin selectivity of α particle evaporation.

Recently, Shimoda *et al.*[10] measured α-HI (heavy ion) coincidences from the $^{12}C(^{16}O,\alpha)$ reaction at $E_{lab} = 142.4$ MeV and found high yields for both α-^{12}C and α-^{16}O coincidences. Moreover, the relative kinetic energy spectra of the α-^{16}O coincidences at different angle pairs showed several peaks which were correlated like those from α-^{12}C. This implies that the sequential α-decay process through $^{20}Ne^*$ resonances also may produce structures in the singles α spectra.

From the various studies, it is clear that there is no direct evidence to substantiate whether or not the $^{12}C(^{16}O,\alpha)$ reaction can populate the molecular resonances with sizable cross section. In the ensuing discussion, we attempt to clarify the origin of the structures in the inclusive spectra. The discussion centers on two experiments, a measurement of the incident energy dependence of the $^{12}C(^{16}O,\alpha)$ reaction, and a coincidence measurement of the $^{12}C(^{16}O,\alpha^{12}C)^{12}C$ reaction. We have already reported our preliminary results on the energy dependence.[11] A similar measurement also was presented by Stwertka *et al.*[12] In the next section, we present a detailed discussion of the measurement of the incident energy dependence. In Sec. III, we describe the coincidence measurement of the $^{12}C(^{16}O,\alpha^{12}C)^{12}C$ reaction. In Sec. IV, we discuss how most of the reported experimental results are understood qualitatively via the sequential α decay of $^{20}Ne^*$ following the α pickup reaction, with possible contributions from the decay of $^{16}O^*$ produced by inelastic excitation. The contributions of the compound process are discussed in Sec. V. A summary of the present work is given in Sec. VI.

II. INCIDENT ENERGY DEPENDENCE OF THE $^{12}C(^{16}O,\alpha)$ REACTION

A. Experimental procedure

The experiments were performed with beams of $^{16}O^{4+}$ and $^{16}O^{5+}$ from the Texas A&M University 224 cm cyclotron at incident energies from 112 to 191 MeV in approximately 10 MeV steps. In the case of the $^{16}O^{4+}$ beam, special care was taken to separate the $^{12}C^{3+}$ contaminant which has nearly the same rigidity as the $^{16}O^{4+}$ ions. The incident beam energies were determined from the calibration of the analyzing magnet, which was obtained via the crossover technique. The uncertainty in the beam energies was estimated to be less than ± 200 keV. The beam was focused on a 160 μg/cm^2 natural carbon target. The ener-

gy loss of the incident beam in the target was estimated to be 450 keV, which is considered sufficient to average over statistical fluctuations in cross sections. The size of the beam spot was kept less than 3 mm in diameter. Because the structures of interest were on a huge continuum background, the effect of beam halo was minimized by careful beam tuning and was checked periodically by using a blank target frame. Average beam currents on target were about 120 nA.

The detection of α particles at $\theta_{lab} = 4°$ was accomplished by using the Enge split-pole magnetic spectrometer with a 120 cm long focal plane detector.[13] A single rectangular slit, which subtended a solid angle of 1.28 msr and an angle of $\pm 1.0°$, was used for a collimation of the spectrometer. To reduce effects of secondary α particles produced by elastically scattered $^{16}O^{6+}$ particles at the entrance window of the focal plane counter, a thin Kapton foil was inserted between the two dipole magnets as a charge stripper. In addition, a thin brass foil was placed just in front of the focal plane counter to stop $^{16}O^{6+}$ elastics that passed through the Kapton foil. The performance of this system was checked by using elastic scattering of ^{16}O on a gold target; the results showed that the influence of secondary α's created by the foils was less than 0.1% of the total yield of α particles and that its spectrum did not have any distinct structure.

In addition, we performed measurements using solid state detectors at incident energies of $E_{lab} = 133 - 154$ MeV in approximately 3 MeV steps both to examine any systematic errors which might have been involved in the magnetic spectrometer measurements and to obtain data at much finer incident energy steps. Each of two counter telescopes set at $\theta_{lab} = 4°$ and $8°$ consisted of a combination of four silicon surface barrier detectors with a 200 μm ΔE, and a total of 4 mm for E. The defining slits for the stacks were 8 and 10 mm in diameter, which corresponded to solid angles of 1.26 and 0.87 msr and angular acceptances of $\pm 1.15°$ and $\pm 0.95°$, respectively. To stop the elastically scattered ^{16}O particles, gold absorber foils were set just in front of the telescopes.

Energy calibrations for the spectrometer were carefully obtained via ^{16}O elastic scattering on a gold target. The α elastic scattering on ^{12}C at $E_{lab} = 79.4$ MeV, was performed to calibrate the counter telescopes. Since it was too time consuming to repeat the beam energy calibrations for all the different incident energies, the calibrations were checked periodically and scaled to the various energies. From detailed investigations of the uncertainties in this procedure, we found that the α-particle energy of the $^1H(^{16}O,\alpha)$ reaction agreed with the predicted value within 150 keV at most incident energies. Since we used the same energy calibration for all different bombarding energy measurements, relative calibration ambiguities were estimated to be less than 100 keV. For both measurements, the overall energy resolution was estimated to be 500 keV, which mainly came from the energy loss in the target.

Conventional electronics and an on-line VAX 11/780 computer were used to obtain the data. Uncertainties in the absolute cross section were estimated to be 20%, which includes uncertainties in the charge collection, target thickness, and detector efficiency.
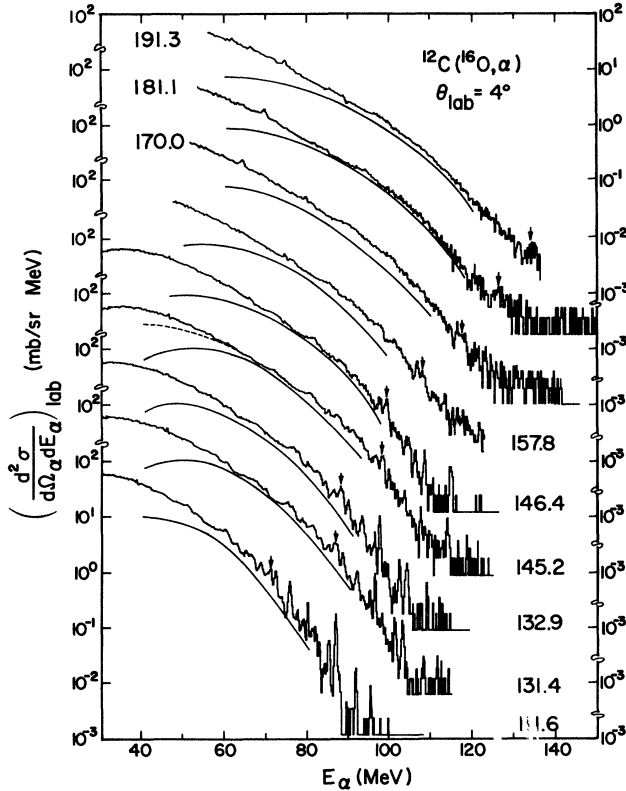
FIG. 1. Inclusive α spectra at various incident energies taken by the spectrometer. Arrows show the $E_x(^{24}Mg)=20.2$ MeV state. The solid and dashed curves are the theoretical spectra obtained by the Hauser-Feshbach code EVA (see the text, Sec. V).

FIG. 2. Background subtracted α spectra obtained by the solid state counter telescope at $\theta_{lab}=8°$. The vertical scalings of the spectra are roughly proportional to differences of incident beam energies shown in the figure. Spurious structures caused by the junction of the solid state detectors are shown by the hatched areas.

B. Experimental results

Inclusive spectra of α particles taken by the spectrometer at several incident energies are shown in Fig. 1. The solid and dashed curves represent the predictions from the Hauser-Feshbach calculations which are discussed in Sec. V. The arrows show the position of the peak at $E_x(^{24}Mg)=20.2$ MeV, which provides a scaling for the excitation energy in these spectra. Over the full incident energy range, huge continuum components are observed in the spectra. On top of the background we can see several distinct structures, especially in the data at lower incident energy. The structures gradually disappear as the incident energy is raised. These results were verified by data obtained with the solid state detector telescopes. The structures are more clearly seen in the background subtracted α spectra. Since we have already reported $\theta_{lab}=4°$ data,[11] only data obtained by the solid state counter telescope at $\theta_{lab}=8°$ are shown in Fig. 2. The method of the background subtraction is the same as described in Ref. 2. The horizontal axis represents the scale of the excitation energies in the ^{24}Mg system, while the vertical axis gives the absolute double differential cross section in the laboratory system with linear scaling. Even though the junction of several solid state detectors caused spurious structures in the spectra, it is obvious that the excitation energies of
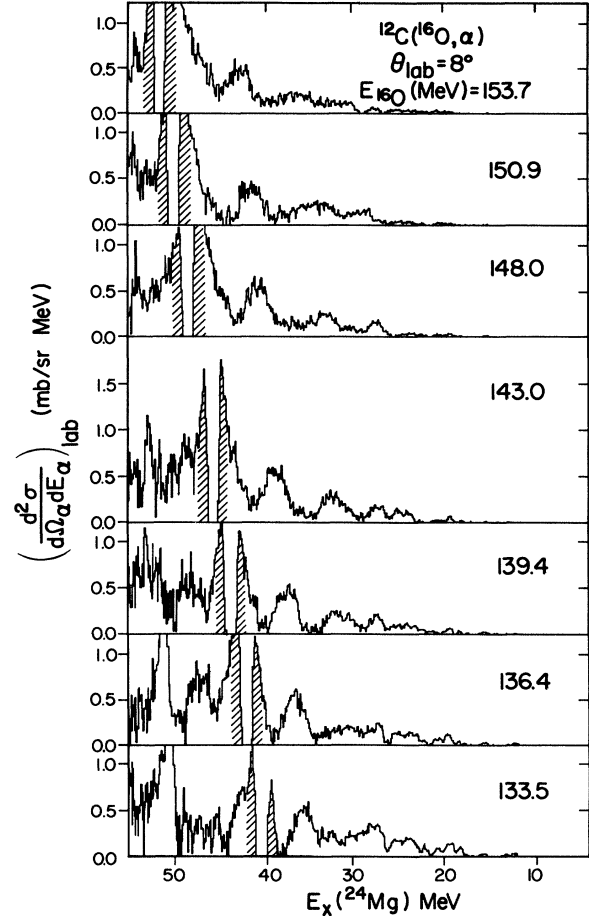
main structures in the "residual" ^{24}Mg system varies continuously as a function of the bombarding energy. This evidently means that most of the structures come from more complicated processes, such as an ejectile sequential α-decay process, than from $^{12}C+^{16}O\rightarrow^{24}Mg^*+\alpha$.

As we pointed out in a previous publication,[11] the movement of the structures in terms of the ^{24}Mg excitation as a function of the incident energy is well explained by sequential α-decay processes from $^{20}Ne^*$ and/or $^{16}O^*$ through the narrow resonances at $E_x(^{20}Ne)=8.8$, 12.0, 14.3, 16.5, 20.5, and 27.0 MeV (Ref. 10) and $E_x(^{16}O)=10.14$, 11.6, 15.8, and 19.4 MeV.[4] The sequential α-decay processes of other ejectiles, such as $^{15}O^*$, $^{17}O^*$, $^{15}N^*$, $^{17}F^*$, $^{12}C^*$, and so on, were also considered by using the simple kinematical calculation described in Ref. 11, but none of them can explain the general tendency seen in the data. Therefore, it seems clear that the $^{20}Ne^*$ and/or $^{16}O^*$ sequential decays play an important role in making the structures. Stwertka et al. also found similar features for these structures, and they suggested that the $^{16}O^*$ sequential decay was a possible origin of them.

III. $^{12}C(^{16}O,\alpha^{12}C)^{12}C$ COINCIDENCE MEASUREMENT

A. Experimental procedure
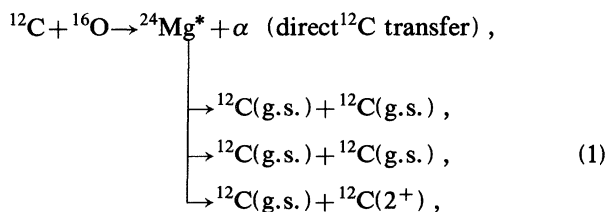
The coincidence measurements were performed with a 146.2 MeV $^{16}O^{4+}$ beam incident on a 480 $\mu g/cm^2$ natural carbon target. The beam energy was estimated to be 145.5 MeV at the center of the target. The size of the beam spot was kept less than 3 mm in height and 2 mm in width to minimize ambiguities of detecting angles. The typical beam intensity on target was 100 nA.

Alpha particles were detected by the Enge split-pole magnetic spectrometer with an 86 cm long single-wire gas proportional counter backed by a plastic scintillator (labeled LI). A slit and foil system were used for the LI counter which were essentially the same as those described for the incident energy dependence measurement.
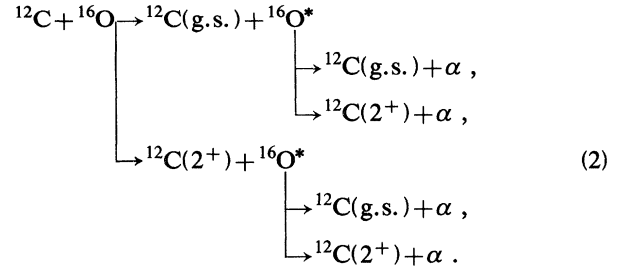
Two silicion surface barrier counter telescopes were used to measure heavy particles. One of them (HI1) consisted of 10.9 μm ΔE, 200 μm E, and 1.5 mm veto counters and the other (HI2) consisted of 16.8 μm ΔE, 200 μm E, and 1.5 mm veto counters. Rectangular defining slits provided for angular acceptances of $\pm 0.5°$, and solid angles of 1.44 and 1.67 msr, respectively. The angular openings of the detection systems and the target thickness were chosen so that the different three-body final states in the $^{12}C + ^{12}C + \alpha$ outgoing channels, $Q = -7.16$, -11.60, and -16.04 MeV corresponding to the ground state, single $^{12}C(2^+)$, and double $^{12}C(2^+)$ excitation, respectively, could be separated at the angles where measurements were performed. For convenience, we represent these three final states by symbols $(0^+,0^+)$, $(0^+,2^+)$, and $(2^+,2^+)$, respectively.

The overall energy resolution in the Q-value scale of the counter telescopes and the spectrometer was approximately 1.2 MeV. This was due mainly to the large angular openings and the energy loss in the target. The energy calibration for the spectrometer was obtained by measuring elastic scattering of ^{16}O on ^{12}C at $\theta_{lab} = 4°$ with several magnetic fields and then fitting those data with a quadratic function. For the telescopes, elastic and inelastic scattering of a 109.6 MeV $^{12}C^{3+}$ beam on a ^{12}C target was used. The total ambiguity in the energy calibrations was estimated to be less than ± 240 keV in all of these counters.

The reaction processes

$$^{12}C + ^{16}O \rightarrow ^{24}Mg^* + \alpha \quad (direct\ ^{12}C\ transfer) ,$$
$$\rightarrow ^{12}C(g.s.) + ^{12}C(g.s.) ,$$
$$\rightarrow ^{12}C(g.s.) + ^{12}C(g.s.) , \qquad (1)$$
$$\rightarrow ^{12}C(g.s.) + ^{12}C(2^+) ,$$

may be obscured by competing processes such as

$$^{12}C + ^{16}O \rightarrow ^{12}C(g.s.) + ^{16}O^*$$
$$\rightarrow ^{12}C(g.s.) + \alpha ,$$
$$\rightarrow ^{12}C(2^+) + \alpha ,$$
$$\rightarrow ^{12}C(2^+) + ^{16}O^* \qquad (2)$$
$$\rightarrow ^{12}C(g.s.) + \alpha ,$$
$$\rightarrow ^{12}C(2^+) + \alpha .$$

The processes (1) and (2) have exactly the same final states, so there is no way to distinguish them by taking coincidence data at only one angular setting. Generally the first reaction steps of processes (2), i.e., inelastic scattering, show quite forward peaked angular distributions. Moreover, their cross sections are likely decreasing as the excitation energy of the ejectile ^{16}O is increasing. On the other hand, the α emission in the processes (1) should have a large yield only at very forward angles while the decay of $^{24}Mg^*$ is not expected to have a very strong angular dependence. These general features imply that if the α and ^{12}C particles are measured at forward angles with a small relative angle separation, the processes (2) might be selectively observed as in the setup of Rae et al.[4] However, if α and ^{12}C particles are measured at very forward and backward angles, respectively, the contribution from the processes (2) should be reduced possibly allowing for the observation of the processes (1). Our measurements were carried out at two such forward-backward angle sets, $\theta_{LI} = 4°$, $\theta_{HI1} = 39.5°$, and $\theta_{HI2} = -34.5°$, and $\theta_{LI} = 4°$, $\theta_{HI1} = 39.5°$, and $\theta_{HI2} = -39.0°$, where the negative angles specify the opposite side of the beam axis from the spectrometer (LI counter). The following additional constraints dictated these geometries. First, the most forward angle for α detection without any instrumental background was $\theta_{lab} = 4°$. Second, the angle corresponding to the perpendicular decay of the ^{12}C from the recoiling $^{24}Mg^*$ provides the largest angular separation between α and ^{12}C, because beyond this angle the undetected ^{12}C has a smaller separation angle from the α particle than the detected ^{12}C in the recoil center-of-mass system. When α particles are detected at $\theta_{lab} = 4°$, the angles for the perpendicular decay of ^{12}C from the recoiling $^{24}Mg^*$ at the 12^+, 14^+, and 16^+ molecular states $[E_x(^{24}Mg) \sim 33, 39, and 47 MeV]$ correspond to $\theta_{lab} \sim 35.7°$ or $-34.6°$, $39.3°$ or $-36.8°$, and $42.7°$ or $-38.7°$, respectively.

Four different types of coincident events, namely LI-HI1, LI-HI2, HI1-HI2, and LI-HI1-HI2, were obtained from the three detection systems. For each coincident event, eight parameters including the event tag, H_ρ, $H_\rho + L_\rho$, $\Delta E(HI1)$, $E(HI1)$, $\Delta E(HI2)$, $E(HI2)$, and the sum of TAC (time-to-amplitude converter) outputs among the three counters, were processed by the VAX 11/780 on-line computer and stored on a magnetic tape event by event for off-line analyses. Here H_ρ and L_ρ denote the two signals from the position wire of the focal plane counter in the spectrometer corresponding to the high and low momentum side, respectively.

The typical coincidence counting rates for LI-HI1, LI-HI2, and HI1-HI2 events were 0.2, 0.1, and 0.3
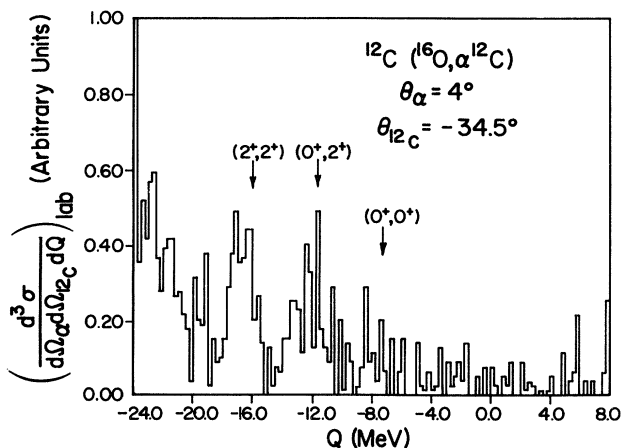
FIG. 3. Typical Q-value spectrum made by using the three-body kinematics. Arrows indicate positions of three different final states, namely the ^{12}C(g.s.)$+^{12}$C(g.s.)$+\alpha$, ^{12}C(g.s.) $+^{12}$C(2^+)$+\alpha$, and ^{12}C(2^+)$+^{12}$C(2^+)$+\alpha$.

counts/sec, respectively, while the single counting rates from LI and HI1 were 2000 and 200 counts/sec.

The accumulated event-by-event data were analyzed off line. Large differences in three-body Q values between ^{12}C $+ ^{12}$C$+\alpha$ and other channels gave us an unambiguous identification of reaction channels, even though the counter systems were not able to provide clear isotope separation. The absolute cross sections were normalized to the singles data in Sec. II, thus the uncertainties were estimated to be 20%.

B. Experimental results

A typical example of the coincidence spectra as a function of Q value is shown in Fig. 3. The ^{12}C $+ ^{12}$C$+\alpha$ final states with Q values -7.16, -11.60, and -16.04 MeV are separated as labeled in the figure. Due to the extremely low counting rates of both true and chance coincident events and the yield ratio of less than 1 to 1 between them, residual counts in the kinematically forbidden region above $Q = -7.16$ MeV are seen. It should be noted that the $Q = -16.04$ MeV peak does not necessarily correspond to the ^{12}C(2^+)$+^{12}$C(2^+)$+\alpha$ final state, because the final states ^{12}C(g.s.)$+^{12}$C(0^+;7.65 MeV)$+\alpha$, and ^{12}C(g.s.)$+^{12}$C(3^-;9.64 MeV)$+\alpha$ have Q values close to this and the energy resolution was not adequate to separate these excitations. For brevity, however, we refer to this peak as (2^+,2^+).

Since we are investigating the three-body final states among the two ^{12}C nuclei (either in their ground and/or excited states) and an α, there are in general three possible pairs of two-body residual interactions which should be distinguished. In the present measurements, the processes (1) and (2) are expected to coexist so that the relative kinematic energies between the detected and undetected ^{12}C particle, the detected ^{12}C and α particle, and the undetected ^{12}C and α particle should be examined to separate these two processes. The final results from the α-^{12}C coincidence data, classified by Q values, are shown in Figs. 4 and 5. The α-^{12}C (undetected) relative kinetic energy spectra are quite similar to the α-^{12}C (detected) spectra shown here, simply because the relative angular separations between α and ^{12}C in both cases are similar as we noted above. To obtain the absolute cross sections in the center-of-mass system of the ^{12}C $+ ^{12}$C $+ \alpha$ three-body system, we used the phase space relation[14]
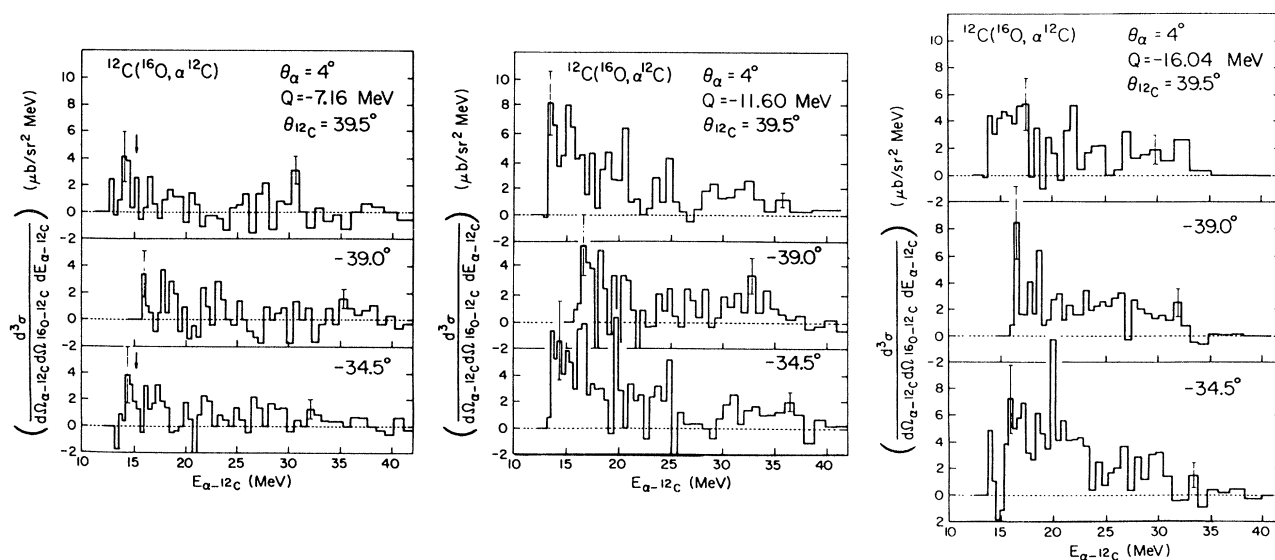

FIG. 4. Triple differential cross sections for the ^{12}C $+ ^{12}$C$+\alpha$ channels in the center-of-mass system of recoil ^{16}O* as a function of the relative energy between the α and detected ^{12}C. Typical statistical errors are shown by the error bars.
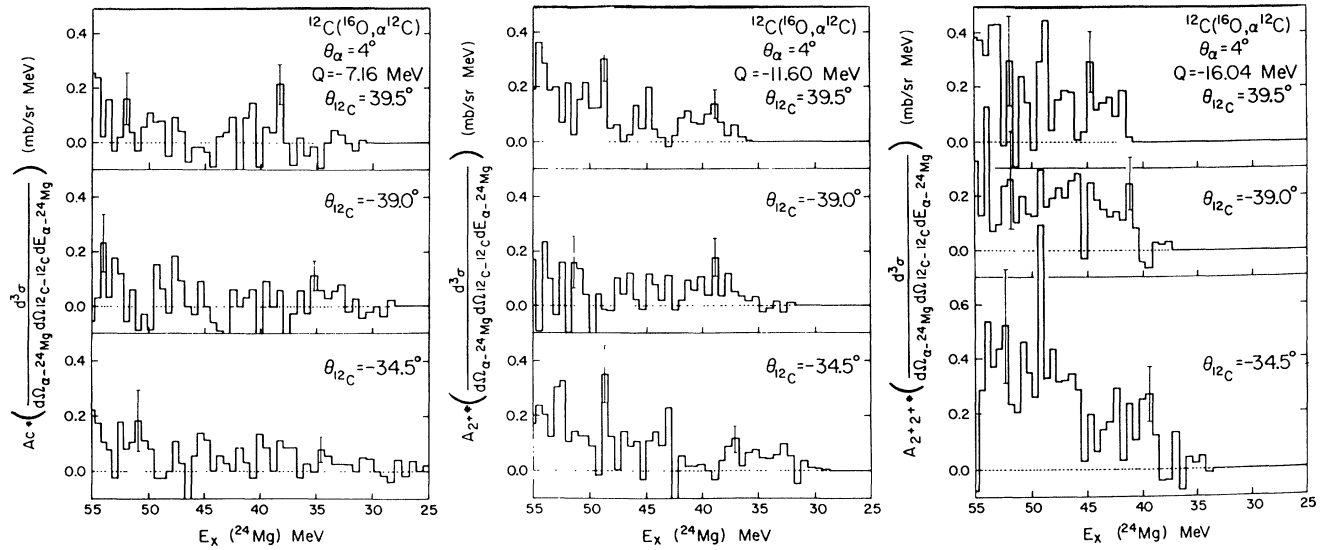
FIG. 5. Triple differential cross sections for the ^{12}C$+^{12}$C$+\alpha$ channels in the center-of-mass system of the recoil ^{24}Mg* as a function of an excitation energy of ^{24}Mg. Typical statistical errors are shown by the error bars.

$$\frac{d^3\sigma}{dE_{ij}d\Omega_{ij}d\Omega_{k-ij}} = \frac{\mu_{ij}\mu_{k-ij}p_{ij}p_{k-ij}}{m_1m_2p_1p_2}\frac{(m_2+m_3)-m_2\vec{P}\cdot\vec{p}_2/p_2^2+m_2\vec{p}_1\cdot\vec{p}_2/p_2^2}{m_3}\frac{d^3\sigma}{dE_1d\Omega_1d\Omega_2} ,$$

with

$$\mu_{ij}=m_im_j/(m_i+m_j) ,$$

$$\mu_{k-ij}=m_k(m_i+m_j)/(m_i+m_j+m_k) ,$$

$$\vec{p}_{ij}=\mu_{ij}(\vec{p}_i/m_i-\vec{p}_j/m_j) ,$$

$$\vec{p}_{k-ij}=\vec{p}_k-m_k\vec{P}/(m_i+m_j+m_k) .$$

The symbols m_i, p_i, E_i, P, and E_{ij} denote the mass, momentum, and energy of particle i; the total momentum; and the relative energy between particles i and j, respectively. Here, 1, 2, and 3 mean the two detected particles and the remaining undetected particle, while i, j, and k refer to any combination of the final three particles.

In order to make direct comparison to the inclusive α spectrum, we renormalize the relative energy spectra between the two ^{12}C particles with the following assumptions. First, all α-^{12}C coincidence events are decays of the nuclear molecular states. Second, the decay angular distributions of the molecular resonances are isotropic in their own rest frame. Third, the decay branching ratios are 0.22, 0.32, and 0.18 for the $(0^+,0^+)$, $(0^+,2^+)$, and $(2^+,2^+)$ channels, respectively. Although there exist no established values for those branching ratios, these ratios have been suggested for the 14^+ state by Cormier *et al.*[15] and similar values have been obtained by Ledoux *et al.*[16] for the 12^+ state by a phase shift analysis. It should be noted that between the energy spectra in the α-^{24}Mg center-of-mass system and relative ^{12}C-^{12}C system there is a difference of a scaling factor, $2m_C/(2m_C+m_\alpha)$, in the absolute cross section. For a direct comparison between

singles α spectra and coincidence spectra, this scaling difference is also included. Finally, the renormalization factors A_C, A_{2^+}, and $A_{2^+2^+}$, for the $(0^+,0^+)$, $(0^+,2^+)$, and $(2^+,2^+)$ channels, are defined as

$$A_i=4\pi\frac{\Gamma_{tot}(2m_C+m_\alpha)}{\Gamma_i 2m_C}(\text{sr}) \quad (i\ ;\ C,\ 2^+,\ \text{and}\ 2^+2^+) .$$

Their actual values are 66.6, 45.8, and 81.4 sr, respectively.

In the α-^{12}C relative energy spectra (Fig. 4), it is hard to identify correlated peaks at different angle pairs, in contrast with the results of the previous coincidence measurement with ^{12}C detectors at relatively forward angles.[4] This is not surprising since our choice of detector angles significantly reduced the available phase space for ^{16}O* breakup processes.

In the relative energy spectra between the two ^{12}C particles, there are few statistically meaningful and correlated peaks, as seen in Fig. 5. This is also demonstrated in the spectra constructed by averaging over the three ^{12}C detection angles 39.5°, $-39.0°$, and $-34.5°$. These are compared to an inclusive spectrum in Fig. 6. In this figure, arrows indicate the cutoff regions of the counter. Even if we assume that all the α-^{12}C coincidence events correspond to the decay of the molecular resonances, their magnitudes are significantly smaller than those of the structures in the singles spectrum. This result depends of course on the angular distribution of the decay process of the ^{24}Mg*. For example, if we assume the decay has a $1/\sin\theta$ angular distribution with respect to the recoil

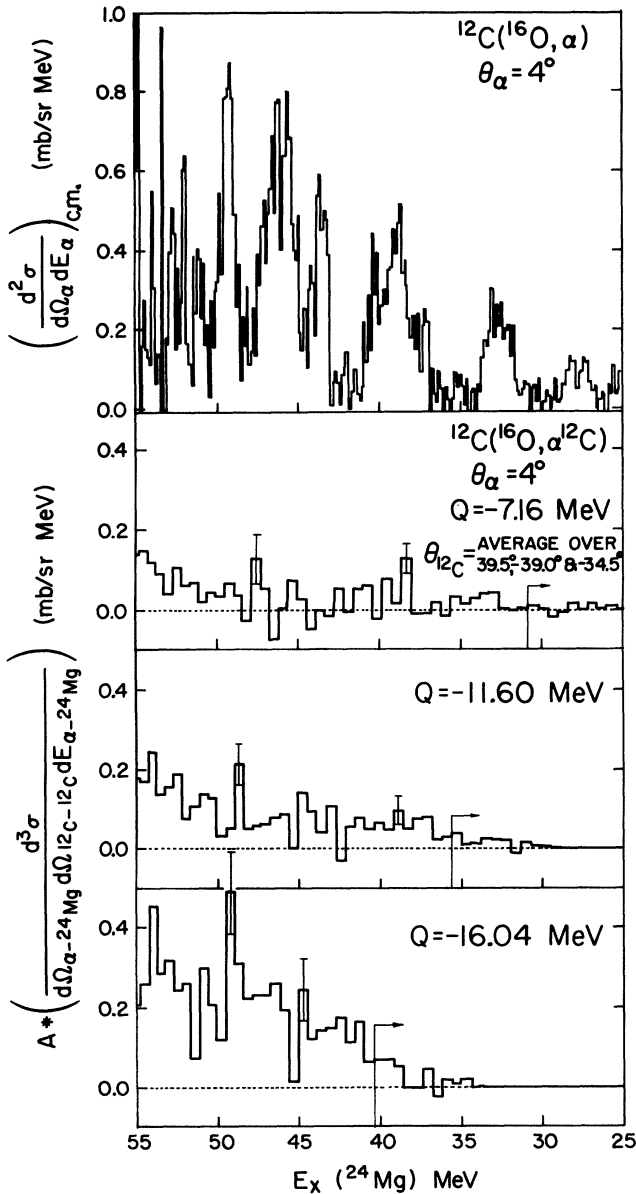FIG. 6. Averaged triple differential cross sections over three observed angles for the $^{12}C+^{12}C+\alpha$ channels in the center-of-mass system of the recoil $^{24}Mg^*$ as a function of excitation energy of ^{24}Mg. Typical statistical errors are shown by the error bars. For reference, the background subtracted singles spectrum obtained by the same detection system is displayed.

direction instead of the isotropic pattern assumed above, the yield ratio between the coincidence and singles becomes approximately 60% larger. But this ratio is still less than one-third. We expect the decays from molecular resonances to be essentially in between these two cases. Two possible explanations of the coincidence data can be offered:

(i) The structures seen in the α inclusive experiments do not originate from the population of $^{12}C + ^{12}C$ molecular resonances.

(ii) The levels in ^{24}Mg populated by a direct ^{12}C transfer

reaction on the ^{12}C target have smaller ^{12}C-decay branching ratio than we expected, and thus do not contribute much to the coincidence yield. A rough estimation of the branching ratios shows that they are less than one-third the values in Refs. 15 and 16.

Our upper limits for the branching ratios are quite consistent with results from a similar experiment by Karp et al. which was published recently.[17] It should be pointed out that since our coincidence detection geometry focused on the highly excited states of ^{24}Mg, we cannot detect decays of molecular resonances in the region below $E_x = 30$ MeV. As for the structures in this energy region, Lazzarini et al.[18] recently claimed that some of them are associated with the $^{12}C + ^{12}C$ resonances.

IV. ALPHA DECAY OF EJECTILES $^{20}Ne^*$ and $^{16}O^*$; ORIGIN OF STRUCTURES ABOVE $E_x(^{24}Mg) = 30$ MeV

Results from the coincidence measurements, along with the observations from the measurements of the singles α spectra as a function of energy, indicate that the dominant structures in the singles spectra are not due to the population of molecular resonances but rather they must arise from other processes. If the sequential processes are responsible, the target dependence of the $(^{16}O,\alpha)$ reaction[6] must originate from differences in the cross sections for producing $^{16}O^*$ and/or $^{20}Ne^*$ from these target nuclei.

The formation of $^{16}O^*$, i.e., inelastic scattering, does not show any strong target dependence.[19] Thus it is difficult to explain the lack of structures in the bombardment of ^{13}C and ^{14}N targets if the $^{16}O^*$ α-decay process significantly contributes to the structure. As for the formation of $^{20}Ne^*$, a difference in yield may come from different cross sections on the α-pickup reaction from various targets.

We performed the $^{16}O(^{12}C,^8Be)^{20}Ne^*$ reaction at $E_{lab}(^{12}C) = 109$ MeV (Ref. 14) in order to compare the formation cross section of $^{20}Ne^*$ in the $^{13}C + ^{16}O$ system to that in the $^{12}C + ^{16}O$ system. The $^{16}O(^{13}C,^9Be)^{20}Ne^*$ reaction, to be compared with the above reaction, was measured by Bradlow et al.[20] at $E_{lab}(^{13}C) = 105$ MeV. Preliminary results from our measurements are reported below. A detailed accounting will be given elsewhere.[21]

In Table I, typical cross sections for the $^{16}O(^{12}C,^8Be)^{20}Ne^*$ reaction at $\theta_{lab} = 10°$ are summarized together with the results of the $^{16}O(^{13}C,^9Be)^{20}Ne^*$ (Ref. 20) and $^{16}O(^{14}N,^{10}B)^{20}Ne^*$ (Ref. 22) reactions. It is recognized that the excitation energies of the states populated by the $^{16}O(^{12}C,^8Be)^{20}Ne^*$ reaction are slightly different from those obtained by the α-^{16}O coincident measurement in the $^{12}C + ^{16}O$ reaction. The excitation energies obtained by the $^{16}O(^{12}C,^8Be)^{20}Ne^*$ reaction are well correlated with those by the $^{16}O(^{13}C,^9Be)^{20}Ne^*$ (Ref. 20) and $^{16}O(^{14}N,^{10}B)^{20}Ne^*$ (Ref. 22) reactions. As seen in the table, it is quite evident that the $^{16}O(^{12}C,^8Be)^{20}Ne^*$ reaction to the states above $E_x = 15.34$ MeV has more than a factor of 5 larger cross section than the other two reactions. Moreover, compared with the $^{16}O(^{13}C,^9Be)^{20}Ne^*$ reaction, the $^{16}O(^{12}C,^8Be)^{20}Ne^*$ reaction is strongly forward peaked. These facts imply that the sequential α-decay process from $^{20}Ne^*$ is a likely origin of the structures; this

TABLE I. Comparsion of α transfer cross sections.

E_x (MeV)	J^π	K^π	$(^{12}C,^8Be)$ 109 MeV 10.0°[a]	$(^{13}C,^9Be)$ 105 MeV 10.0°[b]	$(^{14}N,^{10}B)$ 155 MeV 9.3°[c]
			$d\sigma/d\Omega_{c.m.}$ (mb/sr)		
1.63	2^+	0_1^+	$1.0\pm0.6\times10^{-2}$	$1.8\pm0.3\times10^{-2}$	
4.25	4^+	0_1^+	$5.4\pm1.3\times10^{-2}$	$1.4\pm0.1\times10^{-1}$	4.5×10^{-2}
8.78	6^+	0_1^+	$5.2\pm0.4\times10^{-1}$	$3.0\pm0.2\times10^{-1}$	1.8×10^{-1}
11.95	8^+	0_1^+	$2.4\pm0.3\times10^{-1}$	$1.2\pm0.1\times10^{-1}$	2.0×10^{-1}
15.34	7^-	0^-	$7.9\pm0.5\times10^{-1}$	$1.5\pm0.1\times10^{-1}$	1.3×10^{-1}
21.08	9^-	?	$1.7\pm0.1\times10^0$	$6.4\pm0.6\times10^{-2}$	1.9×10^{-1}
22.87	9^-	?	$9.7\pm0.5\times10^{-1}$		
12.59	6^+	0_4^+	$1.4\pm0.2\times10^{-1}$	$5.4\pm0.5\times10^{-2}$	1.1×10^{-1}
15.88	8^+	?	$6.2\pm0.5\times10^{-1}$	$9.1\pm0.8\times10^{-2}$	1.3×10^{-1}
17.30	8^+	?	$9.7\pm0.6\times10^{-1}$	$8.2\pm1.2\times10^{-2}$	1.3×10^{-1}

[a]This work.
[b]Reference 20.
[c]Reference 22. The errors were not estimated.

process also would explain the lack of structure observed in the $^{13}C(^{16}O,\alpha)$ and $^{14}N(^{16}O,\alpha)$ reactions.

To further test these ideas, we have attempted to calculate the magnitudes of the structures induced in the inclusive α spectra due to sequential processes. For this purpose, we first calculated $\theta_{lab}=4°$ spectra of α particles

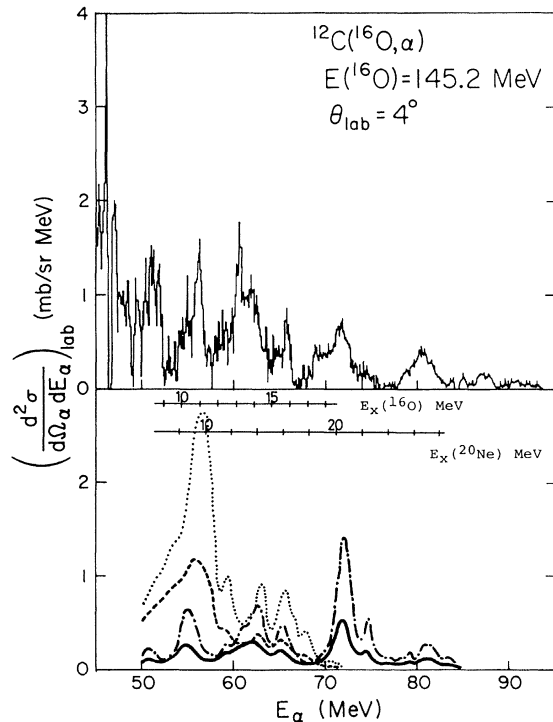FIG. 7. Calculated alpha spectra due to the sequential α decay of $^{20}Ne^*$ and $^{16}O^*$ based on the coincidence data. The solid and dotted-dashed curves correspond to the isotropic and $1/\sin\theta$ α decay of $^{20}Ne^*$, respectively. The dashed and dotted curves represent the isotropic and $1/\sin\theta$ α decay of $^{16}O^*$, respectively.

coming from the $^{16}O^*$ and $^{20}Ne^*$ sequential decay processes at $E_{lab}=145.2$ MeV based on the α-^{12}C and α-^{16}O coincident data obtained by Shimoda *et al.*[10] We assumed the decay of $^{16}O^*\rightarrow{}^{12}C+\alpha$ and $^{20}Ne^*\rightarrow{}^{16}O+\alpha$ to be isotropic in their own frames and integrated the coincidence data over all ^{12}C and ^{16}O directions. Since the angular correlation data covers only a small fraction of 4π, the integration was performed by interpolating and extrapolating the available data into the recoil center-of-mass system of the $^{16}O^*$ and $^{20}Ne^*$ via quadratic and exponential functions whose slopes were determined from the actual angular distributions of the $^{16}O(^{12}C,^8Be)^{20}Ne^*$ reaction. Also calculations were performed using the assumption that the angular distribution of the α decay is axially symmetric about the recoil direction of the $^{16}O^*$ and $^{20}Ne^*$ but follows the form

$$f(\theta)=1/\sin5° \quad \text{for } \theta<5° ,$$

$$=1/\sin\theta \quad \text{otherwise} ,$$

with respect to the recoil direction. The results of the calculations are shown in Fig. 7 along with the background subtracted singles α spectrum. As seen in this figure, the structures due to the sequential α-decay processes of $^{16}O^*$ and $^{20}Ne^*$ have the same order of magnitude predicted yield as the structures in the singles spectra, though the functional forms used for the α-decay angular distributions from the ejectiles can cause quite large changes in the absolute cross section. The structures around $E_\alpha\sim71$ and 80 MeV seem to be due to the sequential α decay of $^{20}Ne^*$ through the narrow resonances at $E_x(^{20}Ne)\sim21$ and 27 MeV, respectively. The peak around 56 MeV probably comes from the sequential α decay of $^{16}O^*$ through the $E_x(^{16}O)\sim11$ MeV state. The other structures likely are due to a combination of the two sequential decay processes.

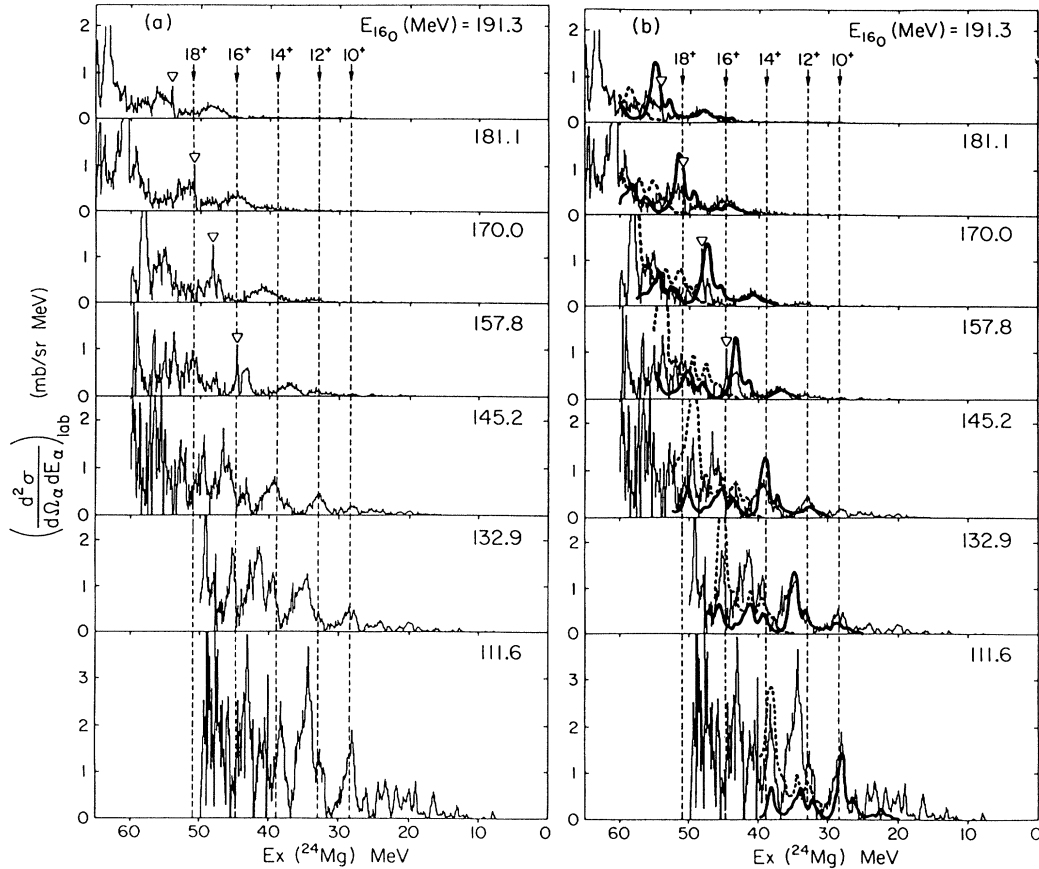We now attempt to explain the incident-energy dependence data following the same procedure. The $^{20}Ne^*$ and

FIG. 8. (a) Alpha spectra at various incident energies; (b) same spectra together with the sequential α decay of ^{20}Ne* and ^{16}O*. The solid and dashed curves correspond to the $1/\sin\theta$ α decay of ^{20}Ne* and ^{16}O*, respectively.

^{16}O* formation cross sections at $E(^{16}O)=112-191$ MeV are not known, we thus assume that their cross sections are constant and equal to those at $E(^{16}O)=142.4$ MeV. In the calculations, the $1/\sin\theta$ angular dependence is used for the α-decay distribution from the ejectiles. The calculated results are shown in Fig. 8(b) together with the background subtracted singles α spectra at $\theta_{lab}=4°$. To make the comparison between experimental and calculated spectra easy, the data from the incident energy dependence are displayed in Fig. 8(a). It should be noted that the kinematical behavior of the structures is well reproduced by the ^{16}O* and ^{20}Ne* sequential α-decay processes.

Also, the angular distributions of the structures were examined using the same calculation. In Fig. 9, the calculated results are compared with the $\theta_{lab}=4°$, 8°, 12°, and 16° α spectra at $E_{lab}=148.0$ MeV obtained by the solid state counter telescopes. The ^{20}Ne* sequential decay process clearly explains the rapid decrease of the cross section with angle and the small variations of the peak positions.

As discussed above, the kinematical features and the magnitudes of the structure observed in the $^{12}C(^{16}O,\alpha)$ reaction are well described by the ^{20}Ne* and ^{16}O* sequential α-decay processes. The remaining puzzle is the target dependence of the structures. To study this, we have calculated the strength of the structures in the $^{13}C(^{16}O,\alpha)$, $^{14}N(^{16}O,\alpha)$, $^{16}O(^{16}O,\alpha)$, and ^{20}Ne$(^{16}O,\alpha)$ reactions coming

from those two sequential processes. The ^{16}O* and ^{20}Ne* formation cross sections on the various targets are not well known. We have assumed that the ^{16}O* cross section is constant. The ^{20}Ne* formation cross sections on the ^{13}C and ^{14}N targets are assumed to be $\frac{1}{5}$ of those on the ^{12}C target following the experimental results summarized in Table I.

The calculated results are shown in Fig. 10 together with the target dependence data of the $(^{16}O,\alpha)$ reactions from Ref. 6. In the cases of the ^{16}O and ^{20}Ne targets, the positions, magnitudes, and shapes of the structures are well explained by the sequential α-decay process of ^{20}Ne*, while the ^{16}O* α-decay process mainly contributes to the background. On the other hand, in the cases of the ^{13}C and ^{14}N targets, the ^{20}Ne* decay process predicts only small structures whose magnitudes are similar to those of the irregularities in the experimental spectra, but the results for the α-decay process of ^{16}O* predicts structures that are too large to be substantiated. There are several reasons for this discrepancy. (1) The use of the $1/\sin\theta$ decay angular dependence for the decays from ^{16}O* is just a guess and may not be appropriate. In fact, even in the ^{12}C target case the contribution of this process is overestimated by approximately a factor of 2. (2) The ^{16}O* formation cross section has a sizeable target dependence contrary to our expectation. (3) The combination of (1) and (2). In
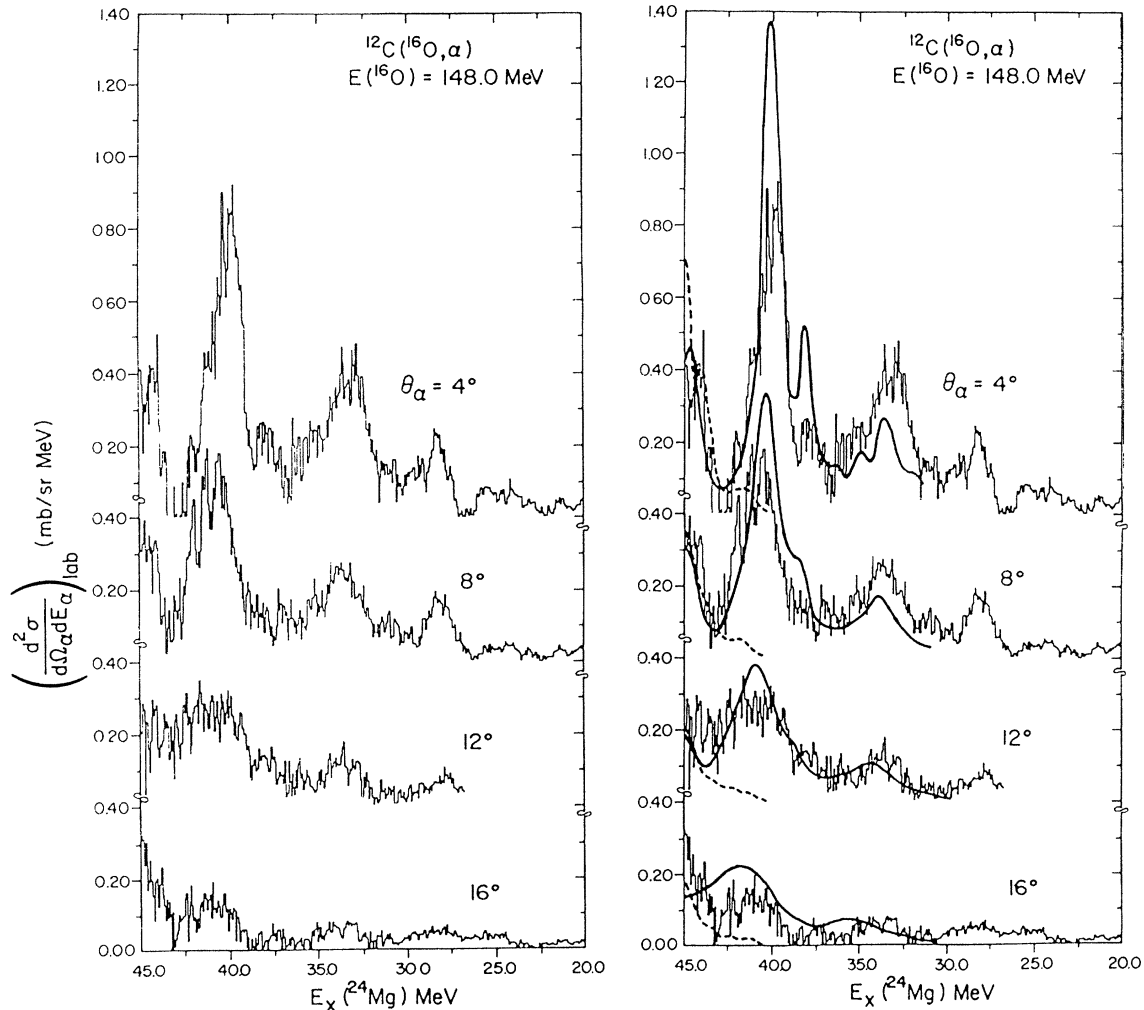
FIG. 9. Angular dependence of alpha spectra due to the sequential α decay of ^{20}Ne* and ^{16}O* together with the experimental data obtained by the solid state counter telescopes. The solid and dashed curves correspond to the $1/\sin\theta$ α decay of ^{20}Ne* and ^{16}O*, respectively.

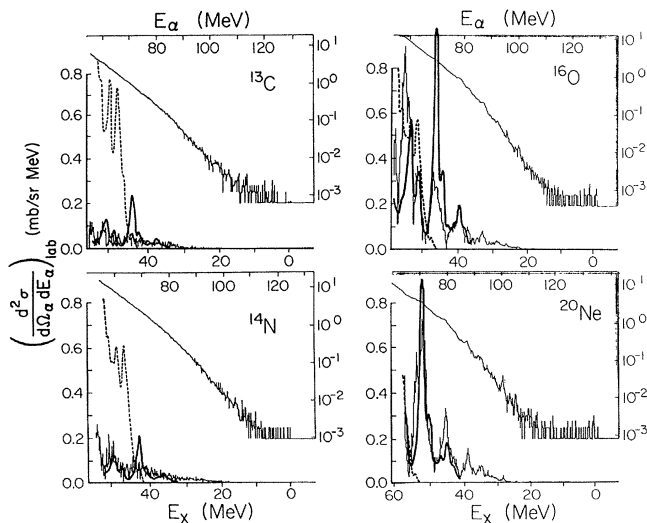FIG. 10. Target dependence of the (^{16}O,α) reactions due to the sequential α decay of ^{20}Ne* and ^{16}O*. The experimental data are from Ref. 6. The solid and dashed curves correspond to the $1/\sin\theta$ α decay of ^{20}Ne* and ^{16}O*, respectively. The details about the assumptions used are described in the text.

order to obtain a reliable explanation, we must examine the singles α spectra of the ^{13}C(^{16}O,α) reaction below $E_\alpha = 60$ MeV, and compare α-HI coincidence data of the ^{12}C + ^{16}O and ^{13}C + ^{16}O reactions. Although there are still some ambiguities, our results strongly suggest that the target dependence of the (^{16}O,α) reactions is mainly coming from the difference of the ^{20}Ne* formation cross section on the various targets.

V. CONTRIBUTION OF COMPOUND PROCESS

A. Origin of the smooth background

As discussed in the previous section, the structures in the $E_x(^{24}$Mg$)=30-56$ MeV range are well described by the sequential α-decay processes. As for the background, we have already reported the Hauser-Feshbach analysis with the experimental result from the ^{14}N(^{14}N,α) reaction.[8] However, recently Cormier *et al.*[9] pointed out that the values of the critical angular momentum for the compound nuclear formation l_c which we adopted for the analysis were not appropriate. Therefore, we have calcu-

TABLE II. Critical angular moment for the ^{16}O+^{12}C system at various incident energies.

E_{lab} (MeV)	111.6	131.4	132.9	145.2	146.4	157.8	170.0	181.1	191.3
l_c (exp)	17	19	19	20	20	20	21	22	22
l_c (th)[a]	18	20	20	21	21	21	22	23	23

[a]For the theoretical calculation by using the statistical yrast line model the parameters $r_0 = 1.15$ fm and $\Delta Q = 12.5$ MeV were used.

lated the contribution from the compound process again with more reliable parameters in order to compare the calculated results with the present data. For this purpose, we modified the Monte Carlo code EVA (Ref. 23) which follows the Hauser-Feshbach formalism. The calculation includes the successive evaporation of neutrons, protons, and α particles. The level densities used are from the prescription of Pühlhofer[24] (we had used the normal Lang formula[25] in the previous work). Pühlhofer's formula is based on the Lang formula in which the effective excitation energy is defined by subtracting the pairing energy and the rotational energy of a rigid rotor from the actual excitation energy. While in the Lang formula all parameters are treated as energy independent, Pühlhofer introduces energy and angular momentum dependent parameters to describe a deformable liquid drop. The parameters used in EVA were obtained from his code CASCADE. For the exit channel, the transmission coefficients were obtained by using a Fermi function,

$$T_l = C_a \{ 1 + \exp[(1 - E_a / B_l)/\Delta] \}^{-1} ,$$

$$B_l = Z_a Z_b e^2 / R_c + [\hbar^2/(2\mu_a)]l(l+1)/R_l^2 ,$$

$$R_c = r_c(A_a^{1/3} + A_b^{1/3}) ,$$

$$R_l = r_l(A_a^{1/3} + A_b^{1/3}) ,$$

where the subscripts a and b refer to three different evaporated particles and the residual nucleus, respectively, and the symbols E, Z, A, and μ denote the energy, charge, mass number, and reduced mass, respectively. The parameters Δ, r_c, and r_l were adjusted to reproduce the transmission coefficients in the α-channel calculated by the optical potential of the α-^{24}Mg system: actual values are $\Delta = 0.1$, $r_c = 1.8$ fm, and $r_l = 1.6$ fm. The normalization factors C_a were chosen to be 0.6, 0.8, and 1.0 for p, n, and α channels, respectively. For the spin cutoff, we calculate the moment of inertia of the residual nucleus using a parameter $r_0 = 1.3$ fm.

The results of the calculations are superimposed on the data in Fig. 1. The solid curves show the results of the first evaporation step, while the dashed curve for the $E(^{16}$O$) = 145.2$ MeV data displays the results of all steps together. As seen from the calculated results of the 145.2 MeV case, most α particles in the region of interest come from the first evaporation step. During the calculations, we tried to adjust the l_c values to fit the experimental data, but no other parameters were changed. Since the number of events in the Monte Carlo calculation were limited, the results have uncertainties of several percent. It is seen that the smooth components of the experimental spectra are well reproduced by the statistical calculation in terms of both shape and magnitude except in the low energy region. The l_c values that we obtained are shown in Table II compared with theoretical ones predicted by using the statistical yrast line model.[26] They show quite good agreement over the entire incident energy range measured. It should be noted that the angular dependence of the background term is also well described by the compounded process as seen in Fig. 11. From these comparisons, we may conclude that the continuum background part is primarily due to the compound process.
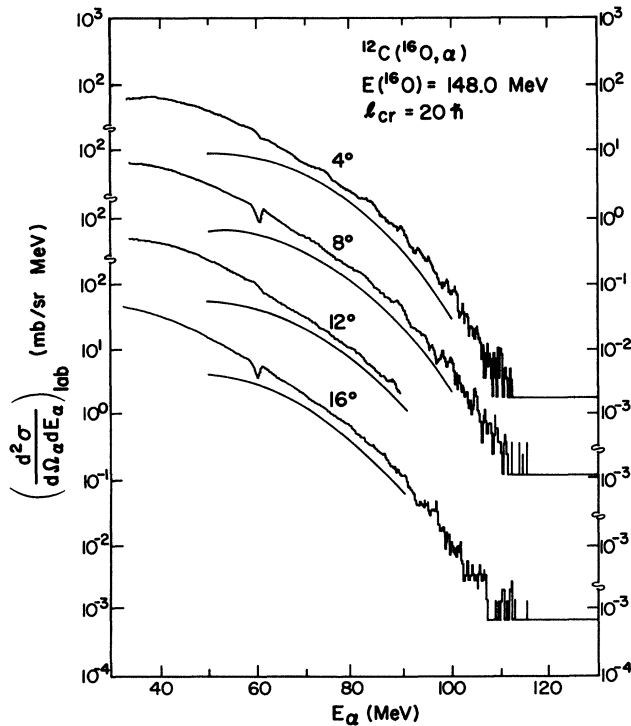

FIG. 11. Angular dependence of the raw α spectra taken by the solid state counter telescopes at $E_{lab} = 148$ MeV. The solid curves are the first evaporation step α spectra obtained by the code EVA with the critical angular moment 20$\hbar$.
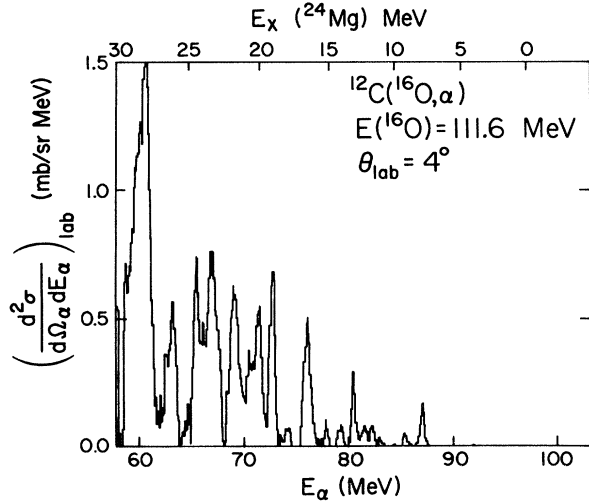
B. Origin of structures below $E_x(^{24}$Mg$) = 30$ MeV

While most of the structures in the region of $E_x(^{24}$Mg$) = 30 - 56$ MeV do not correspond to resonances in ^{24}Mg, those below $E_x = 30$ MeV obviously follow the two-body kinematics of the α-^{24}Mg system. A typical example of the population of the states in ^{24}Mg is shown in Fig. 12. To make the peaks clear, the smooth background

FIG. 12. Typical example of the population of states in ^{24}Mg for the low excitation region at $\theta_{lab}=4°$.

is subtracted in this figure. The members of $K=0^+$, 0^-, and 2^+ bands, for instance, $E_x(^{24}\text{Mg})=1.37(2^+)$, 4.12(4$^+$), 8.12(6$^+$), 13.20(8$^+$), 10.03(5$^-$), 12.45(7$^-$ and 7$^+$), 16.55(9$^-$), 9.52(6$^+$), and 14.11(8$^+$) MeV, are selectively populated in the low incident beam energy cases. However, beyond $E(^{16}\text{O})=157.8$ MeV those states are no longer visible. In the region $E_x=19-30$ MeV, where we could expect to see the nuclear molecular resonances, several states are strongly populated. The energies of those peaks are $E_x=19.2$, 20.2, 20.8, 21.8, 23.5, 24.5, 26.1, and 28.2 (±0.2) MeV, which correlate well to the results of Lazzarini *et al.*[1] (In Fig. 1, the positions of the peak at $E_x=20.2$ MeV are indicated by arrows.)

As for a mechanism of the population of those states, Stwertka *et al.*[12] suggested that compound nuclear formation was likely based on their angular distributions. In fact, some structures, especially the peak around $E_x=28.2$ MeV, appear to consist of several narrow states whose relative intensities strongly fluctuate with incident energy.

To estimate the contribution of the compound process

TABLE III. Level-density parameters (a) a, Δ, β, and E_m and transmission coefficient parameters (b) r_c, E_c, and del$_c$ for the statistical-model calculation.

A_1+A_2	^{24}Mg+α	^{27}Al+p	^{27}Si + n	^{26}Al+d	^{20}Ne+^{8}Be	^{16}O+^{12}C	^{28}Si
a (MeV^{-1})	3.58	3.71	3.71	3.96	3.04	2.18	
Δ (MeV)^c	5.13	1.8	1.8	0.0	5.13	5.13	
β	0.3	-0.1	-0.1	-0.1	0.3	0.0	-0.3
E_m (MeV)^d	9.97	5.25	3.54	3.67	13.33	12.71	
r_c (fm)	1.42	1.25	1.50	1.45	1.63	1.47	
E_c (MeV)	-3.42	-2.34	-0.0	-3.05	-0.37	-2.87	
del$_c$ (%)	8.20	16.3	23.1	15.9	5.10	7.90	

^{a}The level density is

$$\frac{(2J+1)\exp[2(aU)^{1/2}-(J+1/2)^2/2\sigma^2]}{12a^{1/4}(U+t)^{5/4}(2\sigma^2)^{3/2}} \, ,$$

where

$$U=at^2-t=E-\Delta \, ,$$

$$\sigma=(It)^{1/2}/\hbar \, ,$$

and

$$I=2/5mA_I R^2(1+0.31\beta+0.44\beta^2) \, ,$$

with

$$R=1.07A_1^{1/3} \, .$$

$^b T_l(E)=\{1+\exp[(1-E/E_{Bl})/\text{del}_c]\}^{-1}$
where

$$E_{Bl}=\frac{Z_1Z_2e^2}{R_c}+\frac{\hbar^2(l+1/2)^2}{2\mu_c R_c^2}+E_c \, ,$$

$$R_c=r_c(A_1^{1/3}+A_2^{1/3}) \, ,$$

and

$$\mu_c=mA_1A_2/(A_1+A_2) \, .$$

(m =atomic mass unit. Z_1, Z_2, A_1, and A_2 are the charges and masses of the particles in the channel c.)
^{c}Pairing energy.
^{d}Energy above which continuum level densities were used.

to the discrete levels, we carried out a calculation using the Hauser-Feshbach code STATIS.[27] Since the values of l_c predicted by the statistical yrast line model[26] reproduced quite well the continuum background, we used the same values in the calculation. For the distribution of angular momenta, the sharp cutoff model was applied. Six major decay channels n, p, d, α, ^{8}Be, and ^{12}C were included in the calculation. The transmission coefficients for the exit channels were taken to be the Fermi function, whose parameters were adjusted to reproduce the results of optical potential calculations. The optical potential parameters were quoted from Ref. 28. The level densities were also calculated using the Lang formula, whose parameters were taken from Ref. 28. Actual values used for the calculations are listed in Table III. Using these parameters, we can obtain a satisfactory fit to the angular distributions of the ^{12}C(^{16}O,α)^{24}Mg reaction to the ground state in the incident energy range of $E(^{16}$O$)=28.5-100$ MeV.[29] However, in the range of $E(^{16}$O$)=112-191$ MeV, the calculation predicts cross sections for most high-lying states that are at least one order of magnitude too small, even though the structures are assumed to be related to the high-spin members of the ground state rotational band. This discrepancy appears to be too large to attribute to any uncertainties in the experimental or theoretical treatments.

As for the difference between the ^{12}C(^{16}O,α) and the ^{14}N(^{14}N,α) reactions, i.e., the former shows the distinct structures and the latter does not, Cormier *et al.*[9] have calculated the selectivity curves

$$S = \sigma(E_x,I)/\sum_I \sigma(E_x,I)\rho(E_x,I)dE_x ,$$

as a function of the final state excitation energy E_x and spin I using the Hauser-Feshbach formalism. They found that the ^{12}C(^{16}O,α) reaction is $2-4$ times more selective than the ^{14}N(^{14}N,α) reaction for the high spin ($l > 10$) states. However, the states $l > 12$ are expected to appear above $E_x(^{24}$Mg$)=30$ MeV, where the comparison of the two reactions is meaningless since the sequential ejectile α-decay processes are dominant in the ^{12}C(^{16}O,α) reaction. Thus we attempt to discuss the difference between the two reactions in the energy range below $E_x(^{24}$Mg$)=30$ MeV.

The ^{14}N(^{14}N,α) reaction was calculated with the same parameters used for the ^{12}C(^{16}O,α) reaction. Though the predicted cross sections of the ^{14}N(^{14}N,α) reaction to the known discrete states in ^{24}Mg are approximately a factor of 4 smaller than those of the ^{12}C(^{16}O,α) reaction, the selectivity curves S for these two reactions are almost the same for the low spin ($l \leq 10$) states. This fact does not explain the difference between these two reactions, the ^{12}C(^{16}O,α) reaction shows structures and the ^{14}N(^{14}N,α) reaction does not. However, our knowledge about the spins, decay properties, and widths of the structures populated by those reactions is not sufficient to determine whether we have to introduce some sort of a direct reaction process to explain the difference.

VI. SUMMARY

The incident energy dependence measurement of the ^{12}C(^{16}O,α) reaction and the coincidence measurement of the α-^{12}C particles induced by the 145 MeV ^{16}O bombardment of ^{12}C were carried out in order to determine the origin of the structure in the inclusive α spectra from the ^{12}C(^{16}O,α) reaction. Contrary to the previous suggestion, we could not find any evidence for the existence of molecular resonances as final state interactions from ^{12}C(^{16}O,α). The measurement of the incident energy dependence clearly showed that most of the structures in the inclusive α spectra are coming from sequential ejectile α-decay processes. Comparing the ^{12}C(^{16}O,α) and ^{13}C(^{16}O,α) reactions, the ^{20}Ne$^* \rightarrow {}^{16}$O$+\alpha$ process is favorable, since the cross section for the formation of ^{20}Ne* in the ^{12}C $+ {}^{16}$O$\rightarrow{}^{20}$Ne$^* + {}^8$Be reaction is significantly larger than in the ^{13}C $+ {}^{16}$O$\rightarrow{}^{20}$Ne$^* + {}^9$Be reaction. The cross sections of the ^{16}O* formation do not have such a large difference. In fact, using the sequential decay process of the ^{20}Ne*, we can explain the general features of the target dependence of the (^{16}O,α) reactions. On the other hand, we note that the contribution of the ^{16}O* sequential decay process cannot be neglected for the low energy α particles.

The α evaporation from the ^{28}Si compound nucleus accounts for the observed features of the smooth background part of the inclusive α spectra. The absolute cross section, the angular dependence, and the incident energy dependence are well described. However, the Hauser-Feshbach calculations could not reproduce the observed yields to the discrete ^{24}Mg states below $E_x = 30$ MeV.

*Present address: Institute for Nuclear Study, University of Tokyo, Tokyo 188, Japan.
†Present address: Argonne National Laboratory, Argonne, IL 60439.
‡Present address: Department of Physics, University of Tokyo, Tokyo 113, Japan.
§Permanent address: Department of Physics, Tokyo Institute of Technology, Tokyo 152, Japan.

**Present address: Physics Department, National Laboratory for High Energy Physics, Tsukuba, Ibaraki 305, Japan.
[1]A. J. Lazzarini, E. R. Cosman, A. Sperduto, S. G Steadman, W. Thoms, and G. R. Young, Phys. Rev. Lett. **40**, 1426 (1978).
[2]K. Nagatani, T. Shimoda, D. Tanner, R. Tribble, and T. Yamaya, Phys. Rev. Lett. **43**, 1480 (1979).
[3]M. Ichimura, E. Takada, T. Yamaya, and K. Nagatani, Phys.

Lett. B101, 31 (1981).

[4]W. D. Rae, R. G. Stokstad, B. G. Harvey, A. Dacal, R. Legrain, J. Mahoney, M. J. Murphy, and T. J. M. Symons, Phys. Rev. Lett. 45, 884 (1980).

[5]D. Branford, M. J. LeVine, J. Barrette, and S. Kubono, Phys. Rev. C 23, 549 (1981).

[6]N. Takahashi, T. Yamaya, R. Tribble, E. Takada, Y.-W. Lui, D. Tanner, and K. Nagatani, Phys. Lett. B108, 177 (1982).

[7]A. Szanto de Toledo, M. M. Comibra, N. Carlin Filho, T. M. Cormier, and P. M. Stwertka, Phys. Rev. Lett. 47, 632 (1981).

[8]N. Takahashi, E. Ungricht, T. Murakami, Y.-W. Lui, R. Neese, D. Tanner, R. Tribble, and K. Nagatani, Phys. Lett. B110, 445 (1982).

[9]T. M. Cormier, A. Szanto de Toledo, M. M. Coimbra, N. Carlin Filho, P. Stwertka, M. Herman, and N. Nicolis, Phys. Lett. B118, 303 (1982).

[10]T. Shimoda, S. Shimoura, T. Fukuda, M. Tanaka, H. Ogata, I. Miura, E. Takada, M.-K. Tanaka, K. Takimoto, and K. Katori, J. Phys. G 9, L199 (1983).

[11]T. Murakami, E. Ungricht, N. Takahashi, Y.-W. Lui, Y. Mihara, R. E. Neese, E. Takada, D. M. Tanner, R. E. Tribble, and K. Nagatani, Phys. Lett. B120, 319 (1983).

[12]P. M. Stwertka, T. M. Cormier, M. Herman, N. Nicolas, A. Szanto de Toledo, M. M. Coimbra, and N. Carlin Filho, Phys. Rev. Lett. 49, 640 (1982).

[13]N. Takahashi, T. Yamaya, E. Takada, Y.-W. Lui, and K. Nagatani, Nucl. Instrum. Methods 196, 253 (1982).

[14]T. Murakami, Ph.D. thesis, Kyoto University, 1983 (unpublished).

[15]T. M. Cormier, C. M. Jachcinski, G. M. Berkowitz, P. Braun-Munzinger, P. M. Cormier, M. Gai, J. W. Harris, J. Barrette, and H. E. Wegner, Phys. Rev. Lett. 40, 924 (1978).

[16]R. J. Ledoux, M. J. Bechara, C. E. Ordonez, H. A. Al-Juwair, and E. R. Cosman, Phys. Rev. C 27, 1103 (1983).

[17]J. S. Karp, D. Abriola, R. L. McGrath, and W. A. Watson III, Phys. Rev. C 27, 2649 (1983).

[18]A. J. Lazzarini, S. G. Steadman, R. J. Ledoux, A. Sperduto, G. R. Young, K. van Bibber, and E. R. Cosman, Phys. Rev. C 27, 1550 (1983).

[19]C. W. Towsley, P. K. Bindal, K.-I. Kubo, K. G. Nair, and K. Nagatani, Phys. Rev. C 15, 281 (1977).

[20]H. S. Bradlow, W. D. M. Rae, P. S. Fisher, N. S. Godwin, G. Proudfoot, and D. Sinclair, Nucl. Phys. A314, 171 (1979).

[21]T. Murakami, E. Ungricht, Y.-W. Lui, Y. Mihara, E. Takada, and R. E. Tribble (unpublished).

[22]K. Nagatani, C. W. Towsley, K. G. Nair, R. Hanus, M. Hamm, and D. Strottman, Phys. Rev. C 14, 2133 (1976).

[23]E. Ungricht, Texas A&M University Cyclotron Institute Report, 1982 (unpublished).

[24]F. Pühlhofer, Nucl. Phys. A280, 267 (1977).

[25]D. W. Lang, Nucl. Phys. 77, 545 (1966).

[26]S. M. Lee, T. Matsuse, and A. Arima, Phys. Rev. Lett. 45, 165 (1980).

[27]R. G. Stokstad, Yale University, Wright Nuclear Structure Laboratory Internal Report 52, 1972 (unpublished).

[28]L. R. Greenwood, K. Katori, R. E. Malmin, T. H. Braid, J. C. Stoltzfus, and R. H. Siemssen, Phys. Rev. C 6, 2112 (1972).

[29]A. Szanto de Toledo, T. M. Cormier, M. Herman, B. Lin, P. M. Stwertka, M. M. Coimbra, and N. Carlin Filho, Phys. Rev. Lett. 47, 1881 (1981).